Density functional study of photoabsorption in metallic clusters using an exchange-correlation potential with correct long-range behaviour

2002 J. Phys.: Condens. Matter 14 5795

(http://iopscience.iop.org/0953-8984/14/23/311)

INSTITUTE OF PHYSICS PUBLISHING JOURNAL OF PHYSICS: CONDENSED MATTER

J. Phys.: Condens. Matter **14** (2002) 5795–5812 PII: S0953-8984(02)35209-3

Density functional study of photoabsorption in metallic clusters using an exchange–correlation potential with correct long-range behaviour

M B Torres[1] **and L C Balbás**[2]

[1] Dpto de Matemáticas y Computación, Universidad de Burgos, 09006-Burgos, Spain
[2] Dpto de Física Teórica, Universidad de Valladolid, 47011-Valladolid, Spain

Received 26 March 2002
Published 30 May 2002
Online at stacks.iop.org/JPhysCM/14/5795

Abstract

The atomic exchange–correlation (xc) potential with the correct $-1/r$ asymptotic behaviour constructed by Parr and Ghosh (Parr R G and Ghosh S K 1995 *Phys. Rev.* A **51** 3564) is adapted here to study, within time density functional theory, the linear response to external fields of (i) neutral and charged sodium clusters, and (ii) doped clusters of the type Na_nPb ($n = 4$, 6, 16). The resulting photoabsorption cross sections are compared to experimental results, when available, and to results from previous calculations using local and non-local xc functionals. The calculated static polarizabilities and plasmon frequencies are closer to the experimental values than previous results.

1. Introduction

Reliable approximations to the exchange–correlation (xc) functional of density functional theory (DFT) [1] are the keystone for the successful application of DFT to the study of electronic systems. This statement is particularly obviously true when one uses the time-dependent counterpart of DFT (TDDFT) [2, 3] to compute dynamic response properties of finite electronic systems to external exciting fields. The more widely used xc potentials are based on the local density approximation (LDA) [4]. A particularly attractive feature of this approach is its low computational cost, which allows one to treat systems with a large number of electrons. However, a deficiency of the LDA (and likewise of its spin-dependent incarnation [5], LSDA; in the following, we shall drop the distinction) is that it includes a spurious interaction of localized electrons with themselves. The reason for this effect is that the self-interaction contained in the classical Coulomb energy, the Hartree term of the DFT Hamiltonian, is only partially cancelled by the LDA xc energy. The LDA xc potential has the wrong asymptotic behaviour for finite systems: for neutral systems it decreases exponentially at large distance from nuclei, rather than showing the correct $-1/r$ behaviour. This failure originates from the LDA not obeying the so-called 'ionization potential theorem' [6]; that is, the LDA eigenvalue of the highest occupied molecular orbital (HOMO) deviates considerably from the negative of the ionization energy of the system. Another drawback of the erroneous asymptotic LDA

xc potential, which is relevant for the purposes of the present paper, is that the calculated static polarizabilities of metal clusters are about 20% lower than the experimental values [3], although still higher than the classical predictions based on nearly free electrons confined by infinite sharp boundaries [7]. Similarly, TDLDA predictions of the surface resonance frequencies became red-shifted with respect to the classical Mie value [7], but are still blue-shifted with respect to experiments. These errors in TDDFT predictions from using LDA can be traced back to the incorrect long-range asymptotic behaviour of the xc potential, leading to inaccuracies in the virtual orbitals and eigenvalues. In view of this, it is an obvious priority to use a description for the valence electrons leading to single-electron removal energies and excitation spectra more accurate than the LDA predictions [6].

Various efforts have been made to eliminate the self-interaction error in LDA and related density functional schemes. For example, two decades ago, Perdew and Zunger [8] developed methods for the self-interaction correction (SIC) of any energy density functional; correction of the self-consistent one-electron potential follows naturally from the variational principle. Well known outcomes of using SIC are the improvements of the total and xc energies of atoms, accurate binding energies of negative ions, orbital eigenvalues that are close to electron removal energies, improvements of the band gaps of solids, and, more relevant for the purposes of this paper, SIC leads to the correct atomic long-range behaviour of the atomic potential, $\sim -1/r$, and the ground-state electronic density, $\sim e^{-2ar}$ (with $a = (2I)^{1/2}$, where I is the first ionization potential). A different approach for the xc density functional, which is free of self-interaction and exhibits the asymptotic xc potential $\sim -1/2r$ for neutral atoms and clusters, is the weighted density approximation (WDA) [9]. In order to reproduce the $-1/r$ asymptotic behaviour of the exact xc potential, Przybylski and Borstel (PB) [10] introduced a further approximation in the WDA. Aiming to calculate the static polarizability of sodium clusters in the context of the so-called Sternheimer equation, Rubio *et al* [11] introduced an *ad hoc* (WDA-PB) procedure, in which the virtues of both the original WDA and the PB approaches are exploited simultaneously (see below—section 2—for details). The linear response of alkali metal clusters was also obtained by implementing the WDA-PB procedure [12] into the usual TDDFT code, which is a modification of the RPA one given by Bertsch [13]. The PB results in these rather heuristic works are much closer to the experimental values than those obtained using the LDA functional, as a consequence of the improved asymptotic behaviour of the xc potential.

For metallic clusters, the LDA-SIC procedure has been used rather successfully to describe ground-state properties, such as eigenvalues, electron affinities [14], and the static polarizability, as well as the dynamical response properties [15]. The SIC prescription of Perdew and Zunger [8] suffers from the formal difficulty that it leads to orbital-dependent xc potentials and it requires orthogonalization of the spin orbitals at each step to achieve self-consistency. Recent efforts to construct xc potentials which are free of self-interaction effects [16–22] provide a promising alternative for TDDFT applications to the WDA and SIC methods which are more demanding as regards computing requirements. Among the recently constructed potentials, the one given by Parr and Ghosh (PG) [18] represents a more drastic new view of xc effects, where the exchange and the correlation are not considered separately using specific functionals.

In this paper we implement the PG potential in the usual TDDFT code to calculate the electron structure of the ground state, the polarizabilities, and the optical responses of pure and doped sodium clusters. We compare the closeness to experiments of our results for pure sodium clusters with that of the results from recent calculations using two variants of simplified SIC schemes (having in common with ours that they lead to a single non-orbital-dependent xc potential):

(1) the results of [23], using the xc potential of Politis *et al* [19], and
(2) the results of [24], using the method of Krieger, Li, and Iafrate (KLI) [16].

We will also compare our calculated values with those from WDA-PB [11, 12] and SIC [15] types of calculation in order to show that using the PG potential leads to similar improvements with respect to the LDA, but with a smaller computing effort and without further approximations.

The layout of this paper is as follows. In section 2 we present a short description of the PG approximation for the xc potential and we implement it to study the dynamical response within TDDFT, discussing the differences from the LDA, SIC and PB implementations. In section 3 we present and discuss results for the ground-state properties and static polarizabilities of neutral, anionic, and cationic sodium clusters. Section 4 is dedicated to a comparative study of the photoabsorption cross sections of these neutral and charged clusters as described by the present and other TDDFT implementations [12, 15, 22, 23]. The ground state and the response properties of doped Na_nPb ($n = 4$, 6, 16) clusters are studied in section 5, assuming the ionic structure provided by previous calculations [25]. In section 6, a summary is given and future work addressed.

2. Theory

2.1. The Parr and Ghosh approximation

Within standard DFT, the density of an N-electron system $n(\boldsymbol{r})$ in its ground state is given by

$$n(\boldsymbol{r}) = \sum_{i=1}^{N} |\psi_i(\boldsymbol{r})|^2 \tag{1}$$

where the single-electron orbitals $\psi_i(\boldsymbol{r})$ are obtained from solving the Kohn–Sham (KS) equations (Hartree atomic units will be used unless explicitly indicated):

$$[-\tfrac{1}{2}\nabla^2 + V_{eff}(\boldsymbol{r})]\psi_i(\boldsymbol{r}) = \varepsilon_i \psi_i(\boldsymbol{r}). \tag{2}$$

The effective potential V_{eff}

$$V_{eff}(\boldsymbol{r}) = V_i(\boldsymbol{r}) + V_H(\boldsymbol{r}) + V_{xc}(\boldsymbol{r}) \tag{3}$$

is the sum of the ionic, $V_i(\boldsymbol{r})$, electron–electron (Hartree), $V_H(\boldsymbol{r}) = \int \mathrm{d}\boldsymbol{r}'\, n(\boldsymbol{r}')/|\boldsymbol{r} - \boldsymbol{r}'|$, and xc contributions, $V_{xc}(\boldsymbol{r})$ (which contains all the many-electron effects missing in $V_H(\boldsymbol{r})$). The xc potential is determined as $V_{xc}(\boldsymbol{r}) = \delta E_{xc}[n]/\delta n$ after some approximation is assumed for the xc energy functional, $E_{xc}[n]$, a key ingredient—but unknown—of the DFT. The most widespread approximation to $E_{xc}[n]$ is the one provided by the LDA:

$$E_{xc}^{LDA}[n(\boldsymbol{r})] = \int \varepsilon_{xc}^{hom}(n(\boldsymbol{r}))\, \mathrm{d}^3 r \tag{4}$$

where $\varepsilon_{xc}^{hom}(n(\boldsymbol{r}))$ is the xc energy density of a homogeneous electron gas of density $n(\boldsymbol{r})$, so the xc potential at $\boldsymbol{r}$ in the LDA is given by

$$V_{xc}^{LDA}[n(\boldsymbol{r})] = \left.\frac{\delta \varepsilon_{xc}^{hom}(n(\boldsymbol{r}))}{\delta n(\boldsymbol{r}')}\right|_{n(\boldsymbol{r})=n(\boldsymbol{r}')}. \tag{5}$$

Explicit expressions for $\varepsilon_{xc}^{hom}(n(\boldsymbol{r}))$ can be found in the literature [1]. In this paper we will use the one given by Perdew and Wang [26] and we refer to it as the LDA-PW expression. Although there is ample evidence that LDA is accurate enough for many practical purposes in atomic, molecular, and solid-state calculations, there are problems in which the LDA is not good enough [8, 27]. The LDA can be improved mainly in two respects:

(1) by constructing functionals that not only depend on the local density $n(\boldsymbol{r})$ at point $\boldsymbol{r}$, but also depend on the gradients of the density, which leads to the concept of the generalized gradient approximation (GGA) [27];
(2) by explicitly removing the self-interaction error mentioned in section 1 above.

The LDA xc potential, V_{xc}^{LDA}, as well as most of the popular GGA potentials, fall off too steeply for large r, compared to the exact xc potential which falls off as $-1/r$ for neutral systems [1].

The PG approximation to the xc potential [18] was first constructed for atoms with the aim of removing some deficiencies of the LDA, and is based on a series of seminal papers by Zhao, Morrison, and Parr (ZMP) [28]. These authors have shown how to calculate KS kinetic energies and orbitals, as well as DFT orbital energies, and xc potentials, $V_{xc}^{ZMP}[n]$, starting from accurate ground-state electron densities. They have also shown how to obtain xc energies when exact total energies are known, and that the accurate xc energy functional cannot be local. The scheme used to construct $V_{xc}^{ZMP}[n]$ is based on the Levy constrained-search method [1]. An important conclusion of the analysis of $V_{xc}^{ZMP}[n]$ by PG is that it may be as well to eschew the traditional resolution of the xc potential into exchange plus correlation, in favour of a resolution into two terms:

$$V_{xc}^{ZMP}[n] = V_{xc}^{FA}[n] + V_C[n], \tag{6}$$

both of which contribute many-body corrections to the Hartree electrostatic potential, $V_H[n]$. The first term in equation (6) is the SIC to V_H introduced by Fermi and Amaldi (FA) in 1934 [29]:

$$V_{xc}^{FA}[n] = -(1/N)V_H[n] \tag{7}$$

with N (a parameter, not a functional) being the number of electrons. The FA term ensures that the xc hole correctly normalizes to -1 electrons, a very important condition fulfilled by the LDA and WDA approaches, and guarantees the correct long-range behaviour of the potential, in a natural way [29]. This is a significant improvement over the exponential decay of the LDA. The second term in equation (6), $V_C[n]$, arises from the special constraint used in the ZMP method to minimize the kinetic energy and has been called the *constraint potential*. As stated above, one can compute accurate xc potentials from accurate electron densities following the ZMP procedure [28], and, by subtracting $V_{xc}^{FA}[n]$, the constraint potential $V_C[n]$ is obtained.

From examination of accurate actual curves of $V_C(r)$ for neutral atoms, PG [18] have observed that $V_C(r)$ and $r^2n(r)$ show complementary shell structures: a minimum in $V_C(r)$ tends to correspond to a maximum in $r^2n(r)$. This prompts the hope that the quantity $n(r)V_C(r)$ would be simply related to $n(r)$, by means of a universal functional

$$\Gamma(R) = R(n)\frac{V_C(r)}{V_C(0)} \tag{8}$$

with

$$R[n] = n(r)/n(0). \tag{9}$$

From a plot of $\Gamma(R)$ versus R for the atoms He to Ar, PG (figure 1 of [18]) conclude that $\Gamma(R)$ is a 'nearly' universal function of R, and provide the following expression for $\Gamma(R)$:

$$\Gamma(R) = \frac{[kR - 1 + \exp(-kR)]}{[k - 1 + \exp(-k)]} \tag{10}$$

that fits the accurate existing data for the atoms He to Ar with the value of the parameter $k = 7.5$.

In this paper we will denote the constraint potential $V_C[n]$ entering equation (8) as the PG xc term, which leads to

$$V_{xc}^{PG} = V_C(0)\Gamma(R)/R[n] \tag{11}$$

and is determined, up to a constant $V_C(0)$, as a function of the density $n(r)$. When added to the FA component, it results in a particular construction of the ZMP xc potential that we denote as the Fermi–Amaldi–Parr–Ghosh (FAPG) xc potential:

$$V_{xc}^{FAPG}[n] = V_{xc}^{FA} + V_{xc}^{PG}. \tag{12}$$

Our goal in this paper is to apply this potential to the study of static and dynamical properties of metal clusters by self-consistently solving the associated KS and TDDFT equations. The results will be compared with those arising from LDA and beyond-LDA types of calculation. To this end, we choose to fit $V_C(0)$ of equation (11) in such a way that $V_{xc}^{FAPG}(r=0) = V_{xc}^{LDA}(r=0)$ for each one of the clusters we are dealing with. This allows us to scrutinize the effect of the long-range xc interaction on the optical properties of clusters at low excitation energies, a region where the FAPG and LDA potentials are radically different.

While the variational V_{xc} in the KS equations is equal to $\delta E_{xc}[n]/\delta n$, knowledge of V_{xc}^{FAPG} is not sufficient for accurately determining the xc energy, E_{xc}, and the total energy. According to equation (12) we would have

$$E_{xc}^{FAPG}[n] = -\frac{1}{N}E_H + E_{xc}^{PG}[n], \tag{13}$$

E_H being the Hartree energy, and where $\delta E_{xc}^{PG}[n]/\delta n = V_{xc}^{PG}$. Although a formally exact expression has been given by PG for E_{xc}^{PG} in [18], the same authors have demonstrated [18] that an excellent approximation for practical purposes results if one assumes that $E_{xc}^{PG}[n]$ is a homogeneous functional of degree 1. The result is then

$$E_{xc}^{FAPG}[n] = -\frac{1}{N}E_H + \langle n|V_{xc}^{PG}\rangle \tag{14}$$

and the approximate total energy becomes

$$E = \sum_i \varepsilon_i - (1 - 1/N)E_H \tag{15}$$

where the ε_i are the KS orbital energies.

For the purposes of the present work, the ionic structure optimization is not intended and the xc energy functional is not needed. Rather, it is important to describe well the ground-state electronic density profile and the corresponding structure of single-particle levels. Also we need the functional derivative of V_{xc} with respect to density, which is crucial in TDDFT for calculating the dynamical response function. As for the ionic potential of the KS equations, $V_i(\boldsymbol{r})$ in the effective potential of equation (3), we have employed two different models, one for pure sodium clusters and the other for doped Na_nPb clusters. For Na_n clusters we use the spherical jellium approximation, in which a homogeneous spherical background of positive charge plus a distribution of valence electrons describes a metallic cluster. For the ionic potential of Na_nPb clusters we use the spherically averaged pseudopotential (SAPS) model [30], within the local atomic pseudopotentials of Fiolhais *et al* [31], because this model reproduces well [25] the trends for the observed stability [32] and the main geometrical and electronic features of the first-principles calculations [33] for these clusters. Thus, the FAPG potential can be used to describe accurately the electronic xc effects independently of the underlying ionic model—that is, the jellium model or the local pseudopotentials, where the atomic cores are taken into account. In this paper we compare the new FAPG potential versus other electronic xc approaches using the same description of the ionic distribution. In other works [12, 25, 30] the effects of different ionic descriptions on the electronic properties when the same xc potential is employed have been discussed. The same trends for the changes in going from jellium to ionic pseudopotentials as were found previously are expected to occur when the FAPG potential is used, and only small details, not the main features and peaks, should be modified.

2.2. Dynamical response

The fundamental ingredient for the calculation of the response properties of electronic systems in the TDDFT is the response function $\chi(\boldsymbol{r}, \boldsymbol{r}')$ [2,3]. When the system is under the influence of an external applied field of the following multipolar form:

$$V_{ext}(\boldsymbol{r}, \omega) = V_{ext}^{L}(r) Y_L^0(\hat{r}) \mathrm{e}^{-\mathrm{i}\omega t}, \tag{16}$$

the response function $\chi(\boldsymbol{r}, \boldsymbol{r}')$ is obtained from a Dyson-type integral equation:

$$\chi = \chi_0 + \chi_0 K \chi \tag{17}$$

where χ_0 in the independent-particle response function, and the kernel K is given by adding the functional derivatives of the Hartree and the xc potentials with respect to density:

$$K(\boldsymbol{r}, \boldsymbol{r}') = \frac{1}{|\boldsymbol{r} - \boldsymbol{r}'|} + K_{xc}(\boldsymbol{r}, \boldsymbol{r}'); \tag{18}$$

that is, respectively, the Coulomb term and the, so-called, local field correction, $K_{xc}(\boldsymbol{r}, \boldsymbol{r}')$,

No dependence of K on the frequency ω of the external field is assumed. The independent-particle susceptibility χ_0 is constructed via the eigenvalues ε_i, the wavefunctions $\psi_i(r)$, and the retarded one-electron Green functions G corresponding to the self-consistent effective potential of the ground-state density functional calculation:

$$\chi_0(\boldsymbol{r}, \boldsymbol{r}', \omega) = \sum_{i=1}^{occ} \{\psi_i^*(\boldsymbol{r}) \psi_i(\boldsymbol{r}') G(\boldsymbol{r}, \boldsymbol{r}', \varepsilon_i + \omega) + \psi_i(\boldsymbol{r}) \psi_i^*(\boldsymbol{r}') G^*(\boldsymbol{r}, \boldsymbol{r}', \varepsilon_i - \omega)\}. \tag{19}$$

The dynamical $2L$-polar polarizability $\alpha_L(\omega)$ results from the response function through the relation

$$\alpha_L(\omega) = \int V_{ext}^*(\boldsymbol{r}, \omega) \chi(\boldsymbol{r}, \boldsymbol{r}', \omega) V_{ext}(\boldsymbol{r}', \omega) \, \mathrm{d}\boldsymbol{r} \, \mathrm{d}\boldsymbol{r}'. \tag{20}$$

We will deal in this work with the dipole case $L = 1$, and the corresponding subscript will be dropped. The value of $\alpha_1(\omega)$ for a static field, $\omega = 0$, gives the static dipole polarizability, $\alpha(0)$, which will be considered in section 3 below. On the other hand, the dipole photoabsorption cross section $\sigma(\omega)$ can be obtained from $\alpha(\omega)$ using Fermi's golden rule:

$$\sigma(\omega) = \frac{4\pi\omega}{c} \operatorname{Im} \alpha(\omega) \tag{21}$$

and will be calculated for pure and doped sodium clusters in section 4.

The LDA results in sections 3 and 4 below have been obtained by first calculating the LDA for independent-particle susceptibility χ_0^{LDA} and the local field correction, K_{xc}^{LDA}, then integrating equation (17) to obtain χ^{LDA}, and finally $\alpha^{LDA}(\omega)$ from equation (20). A similar procedure leads to $\alpha^{FAPG}(\omega)$. The FAPG kernel is calculated in this work from the FAPG potential as

$$K_{xc}^{FAPG} = \frac{\partial V_{xc}^{FAPG}[n(r)]}{\partial n(r')} \tag{22}$$

which is a non-diagonal *symmetric* matrix in the coordinates $\boldsymbol{r}$, $\boldsymbol{r}'$, as it should be.

We comment now on previous attempts to include the correct long-range behaviour of the xc potential and the corresponding kernel (local field correction) in TDDFT response calculations. The independent-particle susceptibility was obtained by Pacheco and Ekardt [15] using SIC corrections, and then the screening potential effects contained in the kernel K were considered in two ways:

(1) neglecting SIC, which leads to a diagonal matrix like in the LDA case; and
(2) considering also the orbital-dependent SIC potentials, that is, the full SIC-TDDFT with the correct K^{SIC} kernel.

In other work, Saito *et al* [34] attempted to introduce SIC corrections into the kernel by means of an ad hoc Amaldi-type correction, namely

$$K(\boldsymbol{r}, \boldsymbol{r}') = \frac{N-1}{N} K^{LDA}(\boldsymbol{r}, \boldsymbol{r}') \tag{23}$$

where N is the number of electrons and K^{LDA} is the kernel of the LDA:

$$K^{LDA}(\boldsymbol{r}, \boldsymbol{r}') = \frac{1}{|\boldsymbol{r} - \boldsymbol{r}'|} + \frac{\mathrm{d}V_{xc}^{LDA}}{\mathrm{d}n}\delta(\boldsymbol{r}, \boldsymbol{r}'). \tag{24}$$

We refer the reader to the original paper [34] for details. On the other hand, starting with the PB non-local xc potential, there results a kernel K^{PB} which is not a symmetric matrix [11], unlike the exact $K_{xc}(\boldsymbol{r}, \boldsymbol{r}')$, which must be symmetric. For this reason, in previous works [12] a mixed ad hoc WDA-PB procedure was used. In that approach, χ_0 is first constructed from the one-electron eigenvalues, wavefunctions, and retarded Green functions corresponding to the effective PB potential, which shows the correct asymptotic behaviour; in a second step, the screened response χ is obtained from equation (17) using the kernel of the WDA, K_{xc}^{WDA}, which displays the correct symmetrical behaviour. In contrast of this, the use for TDLDA response calculations of V_{xc}^{FAPG} will be consistent throughout this paper, in the sense that K_{xc}^{FAPG} is constructed from V_{xc}^{FAPG}. These facts—the correct asymptotic behaviour of V_{xc}^{FAPG} and the corresponding symmetrical non-local kernal—modify substantially the structure of the response function $\chi(r, r')$, yielding improved static polarizabilities and photoabsorption cross sections with respect to previous calculations, as we show below.

3. Ground-state properties and static polarizabilities of alkali metal clusters

We consider first the electronic ground state of some neutral (Na_8, Na_{20}, Na_{40}) and charged (Na_9^+, Na_{21}^+, Na_{19}^-) closed-shell sodium clusters. As long as our goal is a systematic comparison of the electronic properties using various xc functionals, we treat the ionic skeleton in the simplest possible way, that is, as jellium spheres with a sharp surface at radius $R = r_s N^{1/3}$, taking the value of $r_s = 3.93\ a_0$ (the radius per electron of bulk sodium).

In this section we will see that, due to the improvement of the asymptotic behaviour of V_{xc}^{FAPG}, the FAPG electronic ground state shows a different energy level structure as compared to the LDA one. Not only are the eigenstates more tightly bound, but also the grouping and ordering of levels become modified with respect to LDA. There are a higher number of bound states, and the gap between the HOMO eigenvalue and the lowest unoccupied molecular orbital (LUMO) becomes wider. These effects lead to higher static dipole polarizabilities and to smaller plasmon resonance frequencies, together with increasing fragmentation of the plasmon, as we will discuss in section 4.

A first insight is gained by directly comparing the behaviour at different distances from the centre of the cluster of the various xc potentials. In figure 1 we plot the KS potentials and self-consistent densities of Na_{20} obtained in this work for two cases, the LDA-PW potential of Perdew and Wang [26], which falls off exponentially as $r \to \infty$, and the FAPG potential, which behaves as $-1/r$ for large r. Also shown are the two components of the FAPG potential, namely the FA term, V_{xc}^{FA}, which reproduces the correct asymptotic behaviour, and the short-ranged PG component, V_{xc}^{PG}, reflecting the shell structure of the system. The FA term's main function is to subtract out the self-repulsion in the Hartree potential, V_H, while the PG

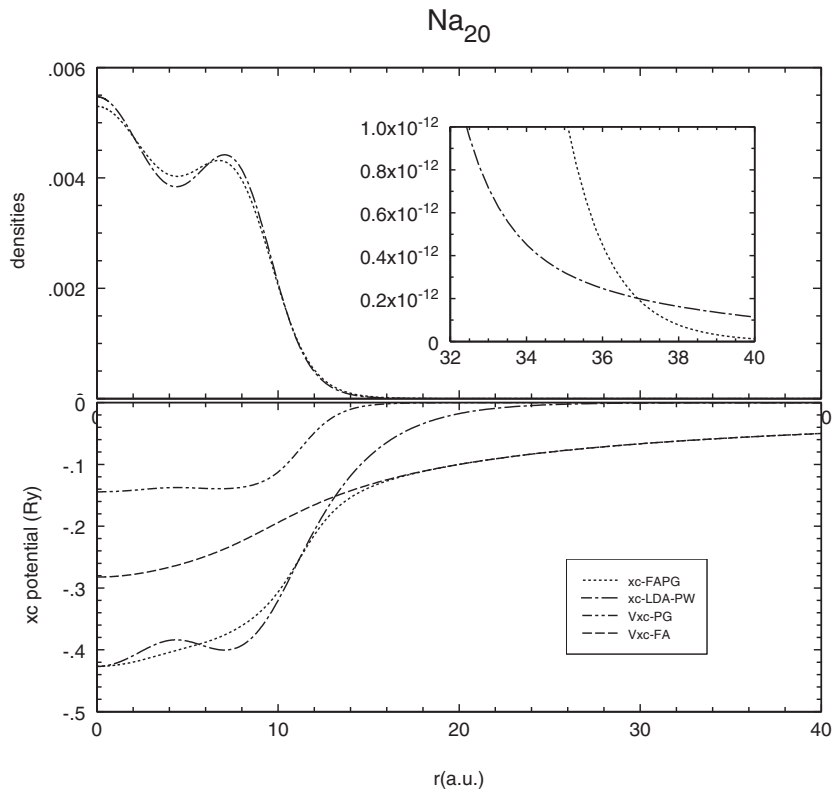

Figure 1. Self-consistent electron densities and KS potentials of Na_{20} in the spherical jellium model, calculated with the LDA (dot–dashed) and FAPG (dotted) approximations. The two components of the FAPG potential are also shown: FA (dashed) and PG (dash–dot–dot).

component is representing correlation plus the interorbital exchange. Note in the inset of figure 1 that the FAPG density is larger than the LDA one from the edge of jellium sphere, $r_{jell} = 10.667$–37 au; that is, the electron spill-out is larger for the FAPG potential than for the LDA. For $r > 37$ au we have the asymptotic regime where the density decays exponentially as $\sim e^{-2ar}$ with $a = (2\varepsilon_{HOMO})^{1/2}$; that is, $\varepsilon^{FAPG}_{HOMO} > \varepsilon^{LDA}_{HOMO}$.

An important consequence is the difference in magnitude between the HOMO eigenvalues obtained in these two approaches. In table 1 we give the ratios of the negatives of the HOMO eigenvalues, calculated using the LDA-PW, FAPG, and PB xc potentials, to the experimental ionization potentials [35, 36], for neutral clusters with 8, 20, and 40 valence electrons. These ratios are closer to unity, the value that exact DFT asserts [6], for the asymptotically correct FAPG and PB potentials than for the LDA one, which severely underestimates the ionization potential.

The orbital energy eigenvalues are a sensitive indicator of the differences between various xc functionals. The different KS eigenvalues and eigenvalue differences resulting from different calculations will drastically affect the linear response of the clusters in the optical region; see section 4 below. It is customary in the vast literature involving LDA calculations to compare orbital eigenvalues with experimental binding energies [37]. For example, in an earlier work using the PB approximation [38], there was a comparison of the eigenvalues of the occupied orbitals with experimental removal energies for noble-gas atoms, which obtained

Table 1. The ratios of the negatives of the HOMO eigenvalues to the experimental ionization potentials for sodium clusters, using different xc potentials. The PB results are taken from [11, 12]. The experimental ionization potentials, I_{exp}, taken from [35, 36] are (in eV) 4.22, 3.76, and 3.58 for the 8-, 20-, and 40-atom clusters.

No of atoms$^{+/-}$	8	20	40
LDA	0.77	0.73	0.76
FAPG	0.92	0.94	0.95
PB	0.96	0.99	1.04

Table 2. Comparison of the KS eigenvalues of the occupied orbitals for a jellium-like Na_{20} cluster obtained with different xc potentials: LDA-PW and FAPG: this work; PB: from [39]; GW: from [40].

Orbital	LDA-PW	FAPG	PB	GW
1s	−5.1	−5.9	−5.8	−5.8
1p	−4.4	−5.2	−5.2	−5.2
1d	−3.4	−4.2	−4.2	−4.4
2s	−2.7	−3.6	−3.7	−3.8

Table 3. The KS eigenvalues (in eV) of the occupied orbitals for the Na_8 cluster in the jellium model, calculated by using different xc approximations: LDA-PW and FAPG: this work; BLYP, KLI, and GAM: from [23]; PB: from [39].

	LDA-PW	BLYP	FAPG	PB	KLI	GAM
1s	−4.53	−4.62	−5.19	−5.30	−5.66	−5.90
1p	−3.27	−3.44	−3.88	−4.04	−4.39	−4.59

excellent agreement. In table 2 we compare the eigenvalues obtained using the LDA and the FAPG potentials for a Na_{20} cluster with the PB eigenvalues [39] and the GW quasi-particle energies obtained in [40]. We see that the xc potentials, FAPG and PB, lead to eigenvalues very close to the GW energies.

Similarly, in table 3 we compare our results for LDA-PW and FAPG 1s and 1p eigenvalues of Na_8 with those resulting from the asymptotically correct xc potentials (KLI [16], GAM [19, 23], and PB [39]), and from the gradient corrected xc potential BLYP [27]. Gradient corrections have a much smaller effect on the orbital eigenvalues than the other non-local approaches. It turns out that the FAPG and PB eigenvalues shift down by ∼0.6 and ∼0.8 eV, respectively, compared to the LDA, whereas the KLI and GAM eigenvalues are much more bound, leading to a negative of the 1p eigenvalue for Na_8 which is much larger than the experimental ionization potential, $I_{exp} = 4.22$ eV. The relative difference in downshift between the individual non-local approximations can be related to the corresponding differences in the xc potential inside the cluster. Thus one finds that the GAM potential is considerably deeper than the LDA one at the centre of the cluster, as can be seen in the figure 1 of [23]. This prompts our selection of the constant V_C in equation (11).

In table 4 we compare, for neutral and charged clusters with 8, 20, and 40 valence electrons, the static polarizabilities calculated with different xc potentials to the experimental values. The static polarizabilities in table 4 are given in units of the classical Mie polarizability, $\alpha_{Mie} = R^3$, where R is the cluster radius, $R = r_S N^{1/3}$, with N = number of atoms, and $r_S = 3.93\ a_0$ is the radius per electron of bulk sodium. The FAPG results as well as the WDA and SIC ones show a systematic improvement with respect to the LDA. This improvement is mainly due to a better description of the external part of the induced density. The WDA-PB and full-SIC

Table 4. The static polarizability in units of the classical Mie polarizability, $\alpha_{Mie} = r_S N^{1/3}$, for neutral and charged sodium clusters with $N = 8$, 20, and 40 valence electrons. LDA-PW and FAPG: this work; PB: from [39]; SIC: from [15]; 'Exp.': experimental values.

No of atoms$^{+/-}$	8	20	40	9^+	19^-	21^+
LDA-PW	1.16	1.15	1.04	1.01	1.31	1.08
FAPG	1.58	1.40	1.30	1.26	1.73	1.27
WDA	1.49	1.42	1.37	1.27	1.72	1.29
WDA-PB	1.81	1.63	1.53	1.48	1.99	1.44
SIC	1.57	1.46	1.41	1.31	1.80	1.33
Full-SIC	1.70	1.61	1.51	1.46	1.80	1.45
Exp.[a]	1.72	1.58	1.56			
Exp.[b]	1.86	1.77	1.55			

[a] Reference [41].
[b] Reference [42].

calculations yield polarizabilities closer to experimental values. Since all calculations reported in table 4 have been performed within the spherical jellium background model, at least a part of the remaining discrepancy with respect to experiment can be ascribed to geometric effects. For a recent discussion of the Na_8 case (and smaller sodium and lithium clusters), see [22].

We are not aware of any experimental determination of the static polarizability for negatively charged clusters, but we can see a systematic enhancement of the FAPG polarizability with respect to the LDA, similar to the findings of other non-local approaches. We would like to point out that, for each group of clusters with a given number of valence electrons, the polarizability is smallest for the cations. This is qualitatively understood in terms of the net confining force with which the ionic background attracts the valence electrons. Because this force is largest in the cations, the electronic density is the more localized, leading to the smallest polarizability.

4. Photoabsorption cross sections of neutral and charged sodium clusters

Recently we have extended the TDLDA framework to study the linear response to spin-dependent external fields and we have applied it to sodium clusters [43]. Here we restricted ourselves to the case of spin-independent fields, but we go beyond the LDA by using the FAPG xc potential and the corresponding non-local xc kernel, equation (22). In figure 2 we show a comparison of the linear TDDFT response to light of interacting valence electrons of Na_{20} and Na_{40} clusters calculated within the LDA-PW (upper panels) and FAPG (lower panels) xc approaches. The dotted lines represent the results for the independent-particle unscreened response and dot–dashed lines correspond to the full response of interacting electrons. The peaks are not delta functions, because we have used a complex photon energy $\omega + i\varepsilon$ with $\varepsilon = 0.02$ eV. The vertical arrow indicates for each case the position of the HOMO eigenvalue in the one-electron spectra.

The multipeaked structure below the ionization threshold appearing in the FAPG response is similar to the one obtained previously within the WDA-PB xc approximation [12]. This increase of strength in the ultra-violet (UV) region is due to the coupling of the collective surface plasmon with one-electron excitations to the loosely bound Rydberg states, which are now properly incorporated in the FAPG spectra. The increase of bound levels in the FAPG with respect to LDA can be seen in figure 2 by simple inspection of the non-interacting spectra, which are composed of simple poles at the electron–hole excitation energies. The strong fragmentation of the FAPG response indicates that no particular transition dominates over the

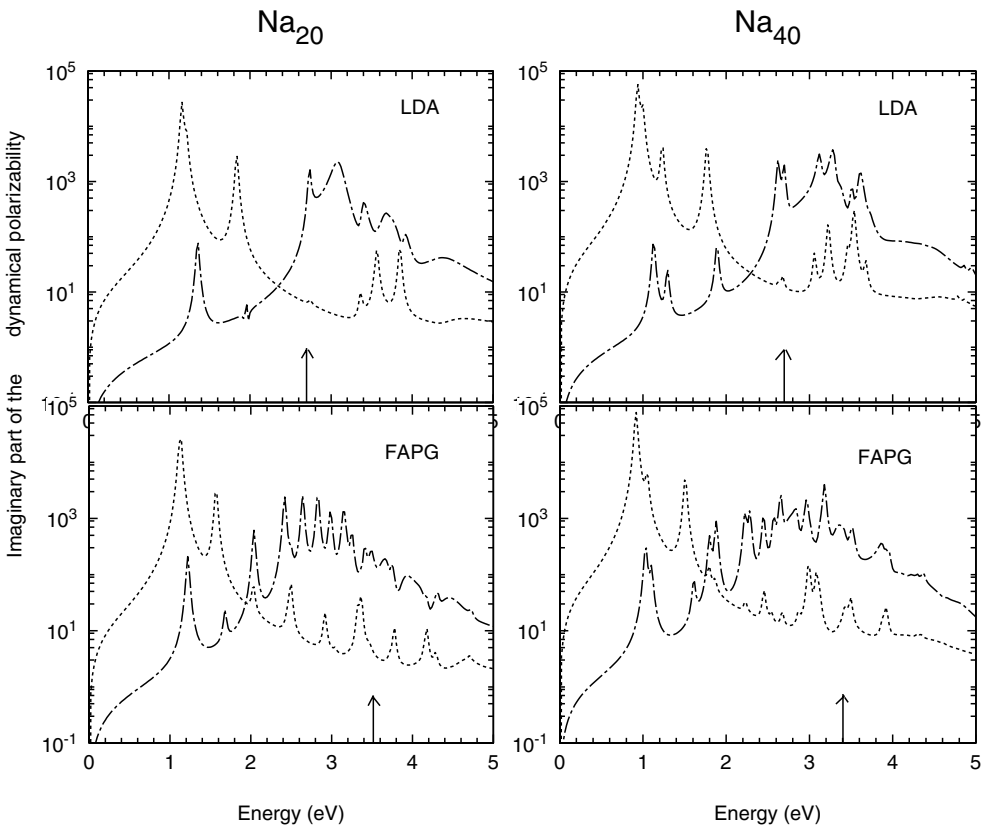

Figure 2. The imaginary part of the dynamical polarizability per electron (on a logarithmic scale and in arbitrary units) for Na_{20} and Na_{40}, versus excitation energy (in eV). The arrow indicates the HOMO eigenvalue. A complex photon energy $\omega + i\varepsilon$ with $\varepsilon = 0.02$ eV has been used.

others, implying a reduction of the total strength in the visible region, which occurs without any significant change in the fragmentation pattern of the collective mode.

A direct comparison of the photoabsorption cross section calculated in the present work with the line shape and linewidth observed experimentally is not appropriate, because of the existence of relaxation mechanisms of plasmon resonance not accounted for at any level of the linear response formalisms considered here. These relaxation mechanisms are responsible for the lifetime of the plasmon, as well as a sizable linewidth associated with the geometry of the ions. The effect of these additional mechanisms can be simulated, in an average way, by folding the calculated cross sections with normalized Lorentzian functions, including damping ratios. Using a Lorentzian width of 0.2 eV (ten times larger than the one used in figure 2) we have obtained two broad peaks (figure 3) which are red-shifted in going from the LDA-PW to the FAPG potential, giving a better agreement with the experimental positions [41], at 2.46 and 2.74 eV for Na_{20} and 2.40 and 2.65 eV for Na_{40}. This qualitative behaviour is the one expected from the results of table 4; that is, the higher the static polarizability, the lower the plasmon frequency. Thus, the FAPG potential leads to an improvement over the LDA predictions of the photoabsorption spectra of sodium clusters. We expect the small shift of the plasmon lines with respect to the experimental observations to be correctable by considering the ionic distribution of the clusters (see [22] for further details).

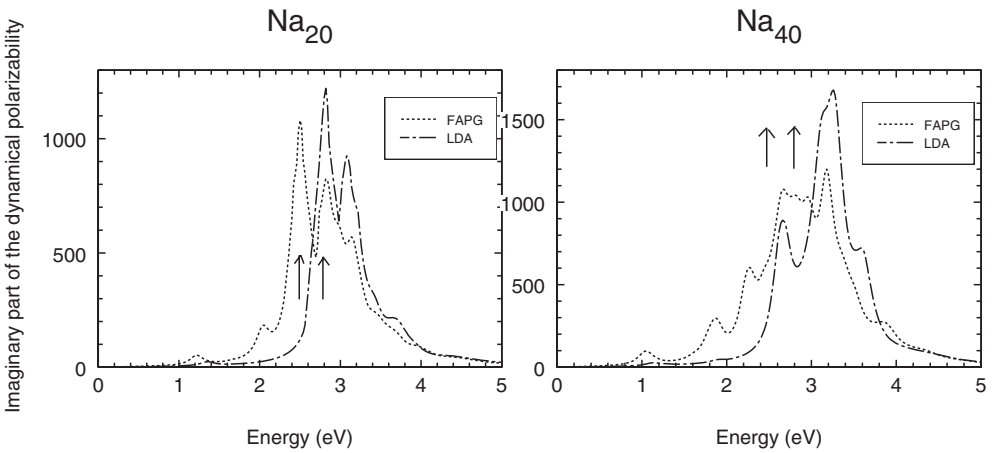

Figure 3. Dipolar responses to light of Na_{20} and Na_{40} clusters calculated within FAPG and LDA descriptions of xc effects. A Lorentzian width of 0.2 eV (ten times larger than in figure 2) is used. Observed peaks are indicated with vertical arrows.

The mechanism of the fragmentation of the plasmon line is not correctly described by the LDA. As an example, in Na_{20} it occurs due to the proximity of the plasmon peak to the particle–hole transition 2s–3p at 2.8 eV. As the 3p level is practically degenerate with the vacuum level, the fragmentation line is broadened due to the proximity of transitions from the 2s level to scattering states. However, the experimental ionization threshold is 3.76 eV (see section 3), and this means that the loss of Rydberg states in the LDA is compensated by the reduction of the ionization threshold. This shortcoming of the LDA becomes corrected in the FAPG case, whose optical spectrum includes the effect of the Rydberg states.

In figure 4 we compare the LDA and FAPG full linear responses (with a Lorentzian broadening of 0.2 eV) of Na_9^+ and Na_{21}^+. The positions of experimental peaks [44] are indicated with arrows. The accumulation of strength in the UV region is smaller for the cations than for neutral clusters because the xc potential is deeper and the overlap between the bound and Rydberg states is smaller. For Na_9^+ we obtain only one FAPG broad peak at an energy very close to the experimental value, 2.62 eV. For Na_{21}^+ a fine structure near the plasmon peak results in the FAPG spectrum, as observed in the experiments [44]. This double peak is absent in both the LDA and SIC [15] spectra, and consequently it is beyond the range of SICs in the xc potential.

The situation is quite different for the negatively charged clusters, where the tail of the potential is now essentially governed by the xc potential, due to the near cancellation of the Coulomb terms. The cross section is now dominated by transitions that promote the electron into the continuum, where it has a finite probability of leaving the cluster. In figure 5 we can observe the large spreading of the strength of Na_{19}^- as compared to its isoelectronic Na_{20} cluster (figure 2). Note as well that the FAPG prediction for the line shape for Na_{19}^- is quite different from the one corresponding to the LDA, showing the importance of correcting for self-interaction and indicating that non-local xc effects should play an essential role whenever the plasmon line is expected to appear near the ionization threshold. Since in the FAPG approach the continuum is treated exactly, the linewidth of the photoabsorption cross section is directly related to the lifetime of the surface plasmon before electron detachment which is delayed compared to that of the neutral cluster. The spreading is also evident in the calculation of Pacheco and Ekardt for Na_7^- and Na_{19}^- [15].

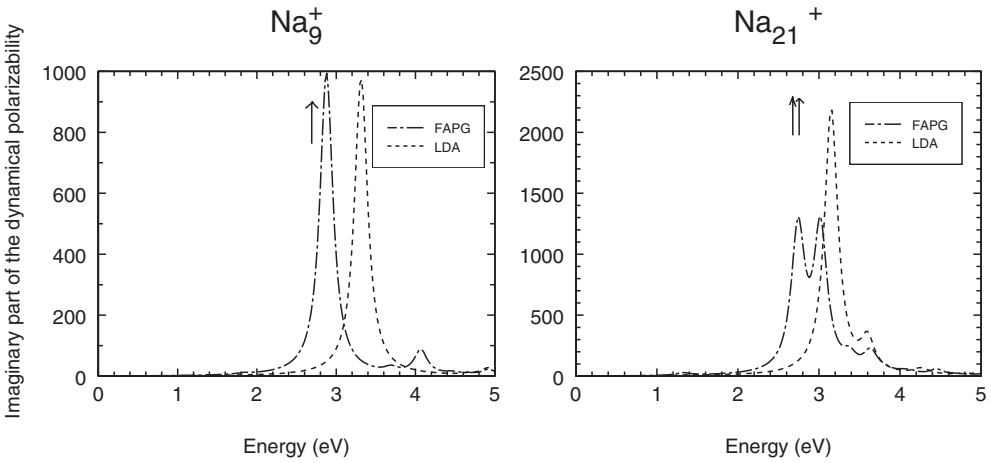

Figure 4. The imaginary part of the dynamical polarizability per electron, for Na_9^+ and Na_{21}^+, calculated with LDA and FAPG potentials. The arrows indicate the positions of the observed peaks [44].

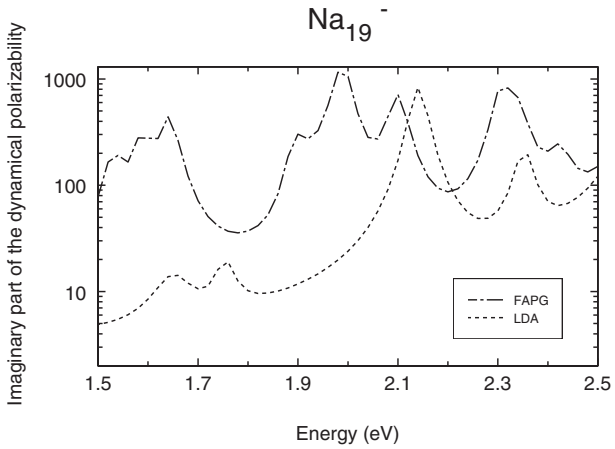

Figure 5. The LDA and FAPG spectra of the Na_{19}^- cluster, to be compared with the isoelectronic spectra of Na_{20} (figure 2) and Na_{21}^+ (figure 4).

5. Ground-state properties and dynamical polarizabilities of Na_nPb clusters

In a mass-spectral study on the stability of bimetallic sodium/lead clusters produced from the expansion of a mixed sodium/lead vapour, an intense molecular beam consisting almost exclusively of the cluster Na_6Pb was observed, under the given experimental conditions [32]. It has been shown, using first-principles molecular dynamics [33], that the strong stability of Na_6Pb comes on one hand from a highly symmetrical configuration formed by a sixfold-coordinated lead atom inside an octahedron, with the six sodium atoms at the vertices, and on the other hand from a closed-electronic-shell structure reminiscent of the $1s^21p^62s^2$ configuration of ten valence electrons in an effective central potential. These circumstances do not exist for the neighbour clusters Na_5Pb and Na_7Pb. The binding energy for the last atom in Na_7Pb

is smaller than the typical binding energies of Na atoms in pure Na clusters, whereas for the smaller mixed clusters the reverse is true. During the process of cluster growth from a Na-rich vapour, it is energetically favourable for a Na atom to bind to a Na_nPb cluster with $n < 6$ instead a pure Na_n cluster, but it is energetically unfavourable for a Na atom to bind to larger mixed clusters instead of a pure Na cluster.

The stabilities of Na_6Pb and other Na_nPb ($n < 23$) doped clusters have been explained [25] by applying the SAPS (spherically averaged pseudopotential) method [30], which is quite successful in predicting the stabilizing of alkali metal clusters by the closing of spherical electronic shells, giving in addition the corresponding optimized skeleton of atomic cores. For the response calculations in this section we start with the ionic geometry resulting from the SAPS method [25] using the local atomic pseudopotentials of Fiolhais *et al* [31] and the LDA-PW xc potential [26] (see [25], chapter 2, for a review). The Pb atom contributes four valence electrons and each Na atom contributes one valence electron. An important feature is that the electronic structure is dominated by the strong attractive Pb potential, resulting in an ordering of electronic levels, 1s1p2s1d—that is, changing the order of the 2s and 1d levels with respect to pure sodium clusters. Thus, electronic shell closure results for Na_4Pb, Na_6Pb and $Na_{16}Pb$. The trends for the stability, cohesive energies, and monomer evaporation energy of Na_nPb clusters obtained in [25] within the SAPS method are the same as those resulting from *ab initio* molecular dynamics calculations [33].

In figure 6 we compare our calculated LDA and FAPG spectra of Na_4Pb, Na_6Pb, and $Na_{16}Pb$. The results for the non-interacting particle response are indicated in figure 6 with dotted lines. The arrows indicate the HOMO eigenvalues. A noticeable increase in the fragmentation of the strength occurs in going from the LDA to FAPG responses, as was discussed above for pure Na clusters.

Let us discuss first the response of the Na_6Pb cluster, whose electronic density is nearly spherically symmetric [33]. For the LDA there are simple poles at 1.39, 2.15, and 3.20 eV corresponding to the particle–hole transitions 2s–2p, 1p–1d, and 1p–3s, respectively. Including the electron–electron interactions, a blue-shift of the response and a broad resonance at 2.6 eV result, although the peak structure already present in the unperturbed response is essentially kept. To analyse what the main transitions contributing to the plasmon peak are, we followed the procedure introduced in [43]; that is, we have made calculations of the response of Na_6Pb, each time keeping inert one of the three occupied sp levels, and comparing it with the full response. The results show that the deeply bound 1s level has little effect on the full response, and the 1p level is responsible for the broad resonance and for the small peak on the right. The 2s level, which is close to the theoretical ionization threshold, causes the remaining structure of the spectrum. As is well known, a local pseudopotential works well for sodium [31]. For lead, this is not so, but the lead atom being placed at the centre should also minimize the role of the non-local parts. Pacheco [45] has shown the great similarity between spectra obtained using local and non-local pseudopotentials and the small influence of the three-dimensional effects in the response of the Na_6Pb cluster.

For the ground state of Na_4Pb in the SAPS model, the p–h transitions are 1p–2s, 1p–1d, and 1p–3s, lying, respectively, at 0.95, 2.08, and 2.55 eV. When we include the induced effective potential, the result is a spectrum that is similar to those of isoelectronic pure sodium clusters with eight valence electrons but shifted globally to higher energies. However, for the $Na_{16}Pb$ case we obtain results that are completely different to those for the isoelectronic Na_{20} and Na_{21}^+ clusters, despite their having the same electronic configuration, $1s^2 1p^6 2s^2 1d^{10}$. The origin of these differences is the strong Pb pseudopotential, causing the 1p and 1d levels to be more tightly bound than in pure Na clusters. This leads also to a blue-shift of the overall spectrum (compare the ranges of energy spanned in figures 2 and 5). On the other hand, the larger

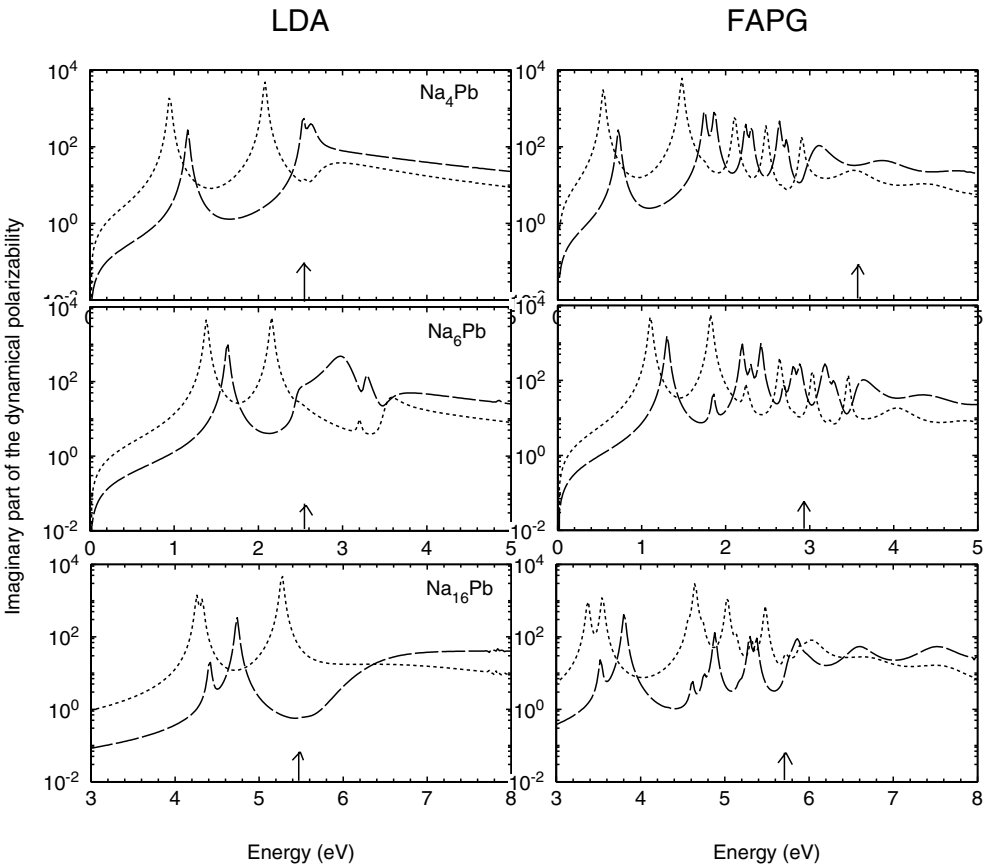

Figure 6. The imaginary part of the dynamical polarizability per electron (on a logarithmic scale and in arbitrary units) for Na_nPb ($n = 4, 6, 16$). The unscreened response is given by dotted lines. The arrows indicate the HOMO eigenvalues.

fragmentation of the FAPG spectra with respect to the LDA spectra is qualitatively similar to the pure clusters case, and the physical origin has been discussed in section 4 above.

6. Summary and outlook

In this paper we have applied DFT to the study of ground-state properties, polarizability, and the photoabsorption cross section for neutral and charged closed-shell sodium clusters as well as sodium clusters doped with lead atoms. The main novel feature is that we treat the xc effects by means of a new xc potential due to PG [18] which exhibits the correct asymptotic behaviour. The use of this new potential in the context of TDDFT provides a simple and convenient framework which does not require extra computational effort and yet yields results that remedy many of the shortcomings intrinsic to the LDA. The FAPG potential of PG [18] eschews the traditional resolution of the xc potential into exchange plus correlation, in favour of a resolution into a FA term plus a constraint term (equation (12)). The former provides the correct normalization of the xc hole and the correct long-range behaviour of the potential, which leads to an increase in the number of bound states. The latter is obtained as a function

of the density by fitting to *ab initio* data for the atoms He to Ar following the procedure of Zhao and co-workers [28]. For the present applications to metal clusters, we choose the value of the FAPG potential at $r = 0$ to be the same as the value for the LDA-PW potential, which we have used here for comparative purposes.

We first considered the ground state of sodium clusters in the spherical jellium model. The HOMO eigenvalue from the FAPG calculations provides a very good account of the ionization threshold. Other FAPG eigenvalues are closer to reported GW quasi-particles energies [40] than those obtained from KLI or GAM potentials [23], which are considerably deeper than the FAPG potential inside the cluster. Moreover, the FAPG approximation yields a better description of the local field correction entering into the response function, leading to a good account of the polarizability, both qualitative and quantitative.

As for the dynamical response properties of sodium clusters, we obtain that the Landau damping is more noticeable in the FAPG calculation than in the LDA one, due to the larger number of loosely bound states. In the case of Na_{20} and Na_{40} we predict accurately the position of the surface plasmon. The observed fragmentation into two main peaks of these plasmons is obtained in both LDA and FAPG calculations, although the underlying mechanisms are different. The fragmentation peak in the LDA is broadened by transitions, promoting the electron into the continuum. In contrast, the fragmentation of the plasmon obtained using the FAPG calculation is due to particle–hole transitions in the discrete spectrum, which now contain much more loosely bound states.

For the positively charged clusters, Na_9^+ and Na_{21}^+, the FAPG calculation provides a red-shift of the main features of the spectra with respect to those from the LDA calculation. For Na_9^+ we obtain only one peak within both FAPG and LDA calculations, but the FAPG one is closer to the experimental plasmon. In the Na_{21}^+ case, only the FAPG calculation reproduces the splitting of the plasmon into two peaks seen in experiments [44]; this has not been obtained using other non-local functionals such as the WDA-PB [12] and SIC [15] forms.

Moreover, we are now able to provide non-trivial predictions for the photoabsorption cross sections of negatively charged clusters. Because the surface plasmon is embedded in a continuum of single-particle states to which it couples within the FAPG approach, we were able to single out the contribution to the total linewidth arising from the probability for electron detachment. This opens the possibility to study previously inaccessible behaviour (at the level of LDA), such as the dynamical response of anions and anionic clusters.

To finish off, in section 5 we studied the linear response of sodium clusters doped with lead atoms and with the ionic structure described by means of the SAPS model [25, 30]. We have calculated and analysed the dynamical response of Na_6Pb within the LDA, obtaining that the 1p level is responsible of the broad resonance near the ionization threshold, whereas the deeply bound 1s level has little effect on the full response. The LDA Na_4Pb spectra are similar to those of the isoelectronic pure sodium clusters Na_8 apart from a global blue-shift due to the strong Pb pseudopotential. Surprisingly, the LDA response of $Na_{16}Pb$ is qualitatively different from that for the isoelectronic Na_{20} cluster, although one should expect a closer correspondence than in the case of eight-valence-electron clusters. Using the PG potential, a noticeable increase in the Landau damping is obtained, as in the case of pure sodium clusters, due to the correct long-range tail.

Acknowledgments

This work was supported by CICYT-Spain (Grant PB98-0368-02) and Junta de Castilla y León (Grant Va 73/02).

References

[1] Hohenberg P and Kohn W 1964 *Phys. Rev.* **136** B864
and for an alternative formulation see
Levy M 1979 *Proc. Natl Acad. Sci., USA* **76** 6062
for a comprehensive account of DFT, see
Parr R G and Yang W 1989 *Density Functional Theory of Atoms and Molecules* (Oxford: Oxford University Press)

[2] Zangwill A and Soven P 1980 *Phys. Rev.* A **71** 1561
For a review of TDDFT see
Gross E K U, Dobson J F and Petersilka M 1996 *Density Functional Theory II (Springer Topics in Current Chemistry vol 181)* ed R F Nalewajski (Berlin: Springer)

[3] Ekardt W, Shone W D and Pacheco J M 1999 *Metal Clusters (Wiley Series in Theoretical Chemistry)* ed W Ekardt (New York: Wiley)

[4] Kohn W and Sham L L 1965 *Phys. Rev.* **140** A1133

[5] von Barth U and Hedin L 1972 *J. Phys. C: Solid State Phys.* **5** 1629

[6] For a recent discussion of the ionization potential theorem see
Perdew J P and Levy M 1997 *Phys. Rev.* B **56** 16 021
Kleinman L 1997 *Phys. Rev.* B **56** 12 042
Kleinman L 1997 *Phys. Rev.* B **56** 16 029
For a discussion of the eigenvalues of unoccupied orbitals see, for example,
Al-Sharif A I, Resta R and Umrigar L J 1998 *Phys. Rev.* A **57** 2466
For a discussion of the eigenvalues of occupied orbitals see, for example,
Baerends E J, Gritsenko O V and Van Leeuwen R 1996 *Chemical Applications of DFT (Am. Chem. Soc. Symp. Ser. vol 629)* ed B B Loird, R B Ross and T Ziegler (Washington, DC: American Chemical Society)

[7] Mie G 1908 *Ann. Phys., Lpz.* **25** 377

[8] Perdew J P and Zunger A 1981 *Phys. Rev.* B **23** 5048
and see also
Svane A and Gunnarsson O 1990 *Phys. Rev. Lett.* **65** 1148
Sen K D and Harbola M K 1991 *Chem. Phys. Lett.* **178** 347

[9] Alonso J A and Girifalco L A 1978 *Phys. Rev.* B **17** 3735
Gunnarsson O, Jonson M and Lundqvist B I 1979 *Phys. Rev.* B **20** 3136

[10] Przybylski H and Borstel G 1984 *Solid State Commun.* **49** 317
Przybylski H and Borstel G 1984 *Solid State Commun.* **52** 713

[11] Rubio A, Balbás L C, Serra Ll and Barranco M 1990 *Phys. Rev.* B **42** 10 950

[12] Rubio A, Balbás L C and Alonso J A 1992 *Phys. Rev.* B **46** 4891

[13] Bertsch G F 1990 *Comput. Phys. Commun.* **60** 247

[14] Penzar Z and Ekardt W 1990 *Z. Phys.* D **17** 69
Stampfi P and Bennemann K H 1989 *Phys. Rev.* A **39** 1007
Madjet M, Guet C and Johnson W R 1995 *Phys. Rev.* A **51** 1327

[15] Pacheco J M and Ekardt W 1992 *Ann. Phys., Lpz.* **1** 254
Pacheco J M and Ekardt W 1992 *Z. Phys.* D **24** 65
Saito S, Bertsch G F and Tománek D 1991 *Phys. Rev.* B **43** 6804

[16] Krieger J B, Li Y and Iafrate G J 1992 *Phys. Rev.* A **46** 5453

[17] Van Leeuwen R and Baerends E J 1995 *Phys. Rev.* A **51** 3564

[18] Parr R G and Ghosh S K 1995 *Phys. Rev.* A **51** 3564

[19] Politis M F, Hervieux P A, Hanssen J, Madjet M E and Martin F 1998 *Phys. Rev.* A **58** 367

[20] Allen M J and Tozer D J 2000 *J. Chem. Phys.* **113** 5185

[21] Stener M, Furlan S and Decleva P J 2000 *J. Phys. B: At. Mol. Opt. Phys.* **113** 5185

[22] van Gisbergen S J A, Pacheco J M and Baerends E J 2001 *Phys. Rev.* A **63** 063201

[23] Ullrich C A, Reinhard P G and Suraud E 2000 *Phys. Rev.* A **62** 053202

[24] Ullrich C A, Reinhard P G and Suraud E 1998 *J. Phys. B: At. Mol. Opt. Phys.* **31** 1871

[25] Torres M B 1997 *Thesis Doctoral* Universidad de Valladolid

[26] Perdew J P and Wang Y 1992 *Phys. Rev.* B **45** 13 244

[27] See, e.g.,
Ernzerhof M, Perdew J P and Burke K 1996 *Density Functional Theory I (Springer Topics in Current Chemistry vol 180)* ed R F Nalewajski (Berlin: Springer) p 1

[28] Zhao Q and Parr R G 1994 *Phys. Rev.* A **50** 2138
Morrison R C and Zhao Q 1995 *Phys. Rev.* A **51** 1980
Zhao Q and Parr R G 1992 *Phys. Rev.* A **46** 2337
Zhao Q and Parr R G 1993 *J. Chem. Phys.* **98** 543
[29] Fermi E and Amaldi E 1934 *M. R. Acad. Italia* **6** 117
[30] Iñiguez M P, López M J, Alonso J A and Soler J M 1989 *Z. Phys.* D **11** 163
[31] Fiolhais C, Perdew J P, Armster S Q, Maclaren J M and Brajczewska M 1995 *Phys. Rev.* B **51** 14 001
[32] Yeretzian C, Röthlisberger U and Schumacher E 1995 *Chem. Phys. Lett.* **237** 334
[33] Balbás L C and Martins J L 1996 *Phys. Rev.* B **54** 2937
[34] Saito S, Bertsch G F and Tománek D 1991 *Phys. Rev.* B **43** 6804
[35] de Heer W A, Knight W D, Chou M Y and Cohen M L 1987 *Solid State Physics* vol 40, ed H Ehrenreich, F Seitz and D Turnbull (New York: Academic) p 93
[36] Kappes M M, Schär M, Röthlisberger U, Yeretzian Ch And Schumacher E 1988 *Chem. Phys. Lett.* **143** 25
[37] See, e.g.,
Selvaraj V and Gopinathan M S 1984 *Phys. Rev.* A **29** 3007
Selvaraj V and Gopinathan M S 1985 *J. Phys. B: At. Mol. Phys.* **18** 3043
[38] Balbás L C, Alonso J A and Borstel G 1987 *Z. Phys.* D **6** 219
[39] Balbás L C, Alonso J A and Rubio A 1991 *Europhys. Lett.* **14** 323
[40] Saito S, Zhang S B, Louie S G and Cohen M L 1989 *Phys. Rev.* B **40** 3643
Saito S, Zhang S B, Louie S G and Cohen M L 1990 *J. Phys.: Condens. Matter* **2** 9041
[41] Selby K, Vollmer M, Masui J, Kresin V, de Heer W A and Knight W D 1989 *Phys. Rev.* B **40** 5417
[42] Tikhonov G, Kasperovich V, Wong K and Kresin V V 2001 *Phys. Rev.* A **64** 063202
[43] Torres M B and Balbás L C 2000 *J. Phys.: Condens. Matter* **12** 4365
[44] Bréchignac C *et al* 1992 *Chem. Phys. Lett.* **189** 28
Ellert C *et al* 1995 *Phys. Rev. Lett.* **75** 1731
[45] Pacheco J M 2001 private communication